Full paper

Role of surface recombination in perovskite solar cells at the interface of HTL/CH₃NH₃PbI₃

Damian Głowienka [a,b,*], Dong Zhang [b], Francesco Di Giacomo [b,c], Mehrdad Najafi [b], Sjoerd Veenstra [b], Jędrzej Szmytkowski [a], Yulia Galagan [b]

[a] *Faculty of Applied Physics and Mathematics, Gdańsk University of Technology, Narutowicza 11/12, 80-233, Gdańsk, Poland*
[b] *TNO – Solliance, High Tech Campus 21, Eindhoven, 5656AE, the Netherlands*
[c] *Centre for Hybrid and Organic Solar Energy, Department of Electronic Engineering, University of Rome Tor Vergata, Via del Politecnico 1, 00133, Rome, Italy*

ARTICLE INFO

ABSTRACT

In order to achieve the highest performance of organometal trihalide perovskite solar cells, it is required to recognize the dominant mechanisms which play a key role in a perovskite material. In the following studies, we have focused on the interfacial recombination between the hole transporting layer (HTL) and the perovskite CH₃NH₃PbI₃ in solar cell devices with p–i–n architecture. It has been shown that Cu:NiOₓ used as HTL drastically decreases a short–circuit photocurrent (J_{sc}) and an open–circuit voltage (V_{oc}). However, we have found that an addition of PTAA thin layer improves cells quality and, as a consequence, the efficiency of such solar cells increases by 2%. Here, we explain both J_{sc} and V_{oc} losses with a theory of the "dead layer" of perovskite material where a very high surface recombination occurs. We demonstrate the numerical and experimental studies by the means of series detailed analyses to get in–depth understanding of the physical processes behind it. Using a drift–diffusion model, it is shown that the presence of a parasitic recombination layer influences mostly the current distribution in the simulated samples explaining J_{sc} and V_{oc} losses. The following results could be useful for improving the quality of perovskite solar cells.

1. Introduction

Hybrid organic-inorganic perovskites attract a lot of attention in the last ten years since the materials started to be used as an absorber in solar cells. With a continuous progress in the field, current state-of-the-art power conversion efficiency (PCE) of perovskite solar cells (PSCs) reached the record value of 24.2% [1]. The outstanding performance of this material is due to a direct band–gap [2], a high charge carrier mobility [3], small exciton binding energy [4] and high absorption co-efficient in a wide spectrum of light [5]. However, the performance of PSCs are still far from the final goal. The theoretical calculations have shown that the highest PCE of PSCs could be around 31% [6]. Although it can be found that the best cells are already reaching a maximum of a short–circuit photocurrent (J_{sc}) [7], there are still observed losses in a fill–factor (FF) and an open–circuit voltage (V_{oc}) related to the recom-bination processes. Therefore, further studies are required to specify which dominant recombination mechanism limits all photovoltaic pa-rameters (J_{sc}, FF and V_{oc}) in order to control them.

In the PSCs, a radiative recombination of charge carriers seems not to play a dominant role in comparison to a nonradiative recombination mechanism [8,9]. The nonradiative recombination takes place when the trapped electron (or hole), which is located at the energy level within the band–gap, recombines with an opposite charge carrier. However, the traps could be mainly accumulated either at the grain boundaries of the polycrystalline perovskite material [10] or at the interface between the perovskite and an electron transporting layer (ETL) or a hole trans-porting layer (HTL) [11]. It seems that both types of accumulation exist in the PSCs and impact the final performance [8,12]. The aim of this work is to investigate and understand the role of recombination pro-cesses which occur at the interface of HTL/perovskite.

In general, an interface recombination is well known to impact the properties of the solar cells [13,14]. However, only recent studies have reported the importance of this type of recombination in PSCs [15–17]. The presence of surface recombination is inherent to a perovskite ma-terial as perovskite crystals grow depending on the quality of the layer which is underneath. Nakane et al. [18] have shown that a growth of the

---

perovskite on TiO_2 could result in the creation of a "dead layer" which is parasitic for the perovskite with a very high recombination, leading to decrease of J_{sc} and, as a consequence, lowering the final performance of PSCs. It seems that, in general, the growth on metal oxide might give raise to lowering of interface quality, while this effect does not occur when growing the perovskite layer on organics. It might be related to the presence of surface defect states in metal oxides which lead to high interface recombination [19]. However, the more likely scenario is that the chemical reaction taking place at the interface of metal oxides causes the formation of recombination layer during the perovskite crystallization process [20,21]. Fortunately, several techniques have been already presented to reduce the surface recombination by e.g. temperature treatment [22], chemical passivation [23,24] or laser treatment [25].

In this work, we explore the idea of surface recombination with the concept of a dead (recombination) layer which appears between $Cu:NiO_x/CH_3NH_3PbI_3$ and has a direct parasitic influence on J_{sc} and V_{oc}, and therefore on the efficiency of PSCs. Also, it is shown that a chemical modification of $Cu:NiO_x$ with PTAA material reduces the parasitic effect in the absorber layer. Further, in order to qualitatively verify the existence of a dead layer and explain its role in the PSC operation, the experimental results with different illumination conditions were used in the simulations. For the simulation purposes, the drift–diffusion model has been applied [26–32]. Finally, we show the influence of different thicknesses and surface recombination velocities on the operation of PSCs.

2. Simulation tool

The drift–diffusion model used in this work describes a generation, transport and recombination of charge carriers for the given PV stack. It also includes continuous equations to quantitatively describe the behavior of electrons and holes, and also the Poisson equation to calculate the electric field in space and time

$$\nabla \cdot F = \frac{q}{\varepsilon_0 \varepsilon_r}(p - n + N_D - N_A),$$ (1)

where F is an electric field distribution, q represents an elementary charge, ε_0 is a permittivity of vacuum, ε_r describes a permittivity of the material, p and n are hole and electron concentrations, respectively. The parameters N_D and N_A represent donor and acceptor concentrations in ETL and HTL layers, respectively. The transport of free charge carriers is governed with the following equations of drift and diffusion currents for electrons

$$J_n = qn\mu_n F + \mu_n k_B T \nabla n,$$ (2)

and for holes

$$J_p = qp\mu_p F - \mu_p k_B T \nabla p,$$ (3)

where k_B is the Boltzmann constant, T represents temperature, and μ_n and μ_p are mobilities of electrons and holes, respectively. More detailed equations for the one dimensional, time–dependent model are included in Supplementary Information (SI). In this study, the surface recombination is not two–dimensional as it is usually assumed. Instead, we take into account the existence of a three–dimensional parasitic layer with the same properties as the absorber. The trap–assisted monomolecular recombination occurs there with the surface recombination rate described by the equation:

$$R_s = \frac{N_t \sigma_s}{\nu_{s,p}^{-1}(n + n_1) + \nu_{s,n}^{-1}(p + p_1)}\left(np - n_{int}^2\right),$$ (4)

where $\nu_{s,n}$ and $\nu_{s,p}$ are the surface recombination velocities for electrons and holes, respectively, N_t represents density of trap recombination centers, $\sigma_s = 1/(N_t L_a)$ is the capture cross section calculated for the absorber thickness L_a, n_1, p_1 and n_{int} are defined with Boltzmann

statistics, see equations (S16)–(S18) (SI).

In the simulation of the PSCs structure, the drift–diffusion model has been extended to simulate both transporting layers (ETL and HTL) [26]. Fig. 1 shows a band diagram of the investigated PSC, with the following layers sequence $ITO/HTL/CH_3NH_3PbI_3/ETL/Au$, where HTL is $Cu:NiO_x$ with or without PTAA, and ETL is PCBM/BCP. In the current study, two variations of HTL so called $Cu:NiO_x$ and $Cu:NiO_x/PTAA$ were used. However, we treat PTAA as a passivation layer, and therefore it is not included in the electrical simulation model. Its influence is visible in the presence of a dead layer which appears only on $Cu:NiO_x$ (Fig. 1(inset)) but not on PTAA passivated layer (Fig. S2 (SI)). The interfaces between the layers in the p–i–n structure lead to numerical difficulties, therefore the change in the permittivity has been included in the Poisson equation [33], see equation (S30) (SI). Also, the energy levels for electron and hole transporting layers are not aligned creating injection barriers (see Fig. 1), which drastically influences the final performance of the solar cell. Therefore the method of generalized potentials [34–36] has been used to include these variations, as shown in equations (S20)–(S21) (SI). The developed model is applicable to any PSCs structure when parameters are well described.

Table 1 shows all parameters (if not specified otherwise) used for the simulation of HTL, ETL and perovskite layer in PSCs. The thickness (L) is an experimental value because each layer was measured with a profilometer. The spatial grid was discretized with Chebyshev polynomials (equations (S8)–(S11) (SI)) reducing the number of grid points (N) needed for fast convergence of numerical simulations. Relative permittivities (ε_r) for ETL and HTL have been calculated from optical η and κ parameters, see Fig. S1 (SI). For the perovskite material, Lin et al. [37] have shown that a dielectric constant is much higher than obtained from ellipsometry measurements, therefore we have decided to use a literature value [38]. Asymmetric mobilities for opposite charge carriers were chosen close to reference values with more mobile electrons ($24\ cm^2\ V^{-1}\ s^{-1}$) than holes ($1\ cm^2\ V^{-1}\ s^{-1}$) [3,39]. Charge carrier capture coefficients ($C_{n(p)}$) used in the Shockley–Read–Hall recombination are close to literature values and they are equal to $5.56 \times 10^{-14}\ m^3\ s^{-1}$ and $4.35 \times 10^{-14}\ m^3\ s^{-1}$ for electrons and holes, respectively [29,40]. The density of traps (N_t) is taken from reference Ref. [29]. The energy trap level has been fixed in the middle of an energy band–gap, which seems to be the most efficient [41]. The bimolecular recombination is based on the Langevin model with reduction prefactor (ξ) adopted from the literature [29]. Although, the Auger recombination is the least
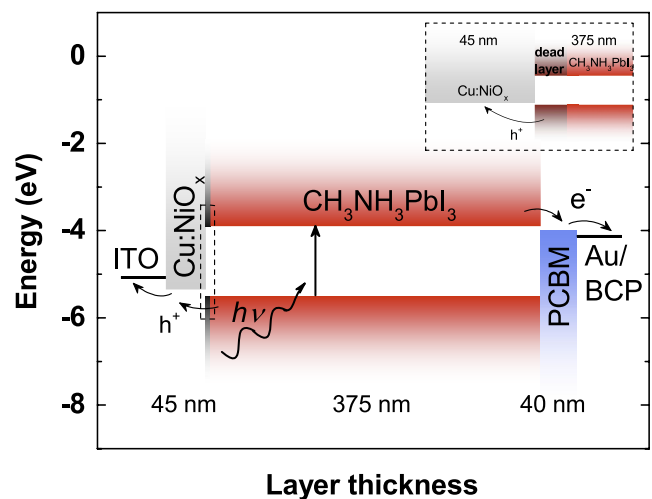

Fig. 1. Device structure of PSC. After photon absorption, free electrons and holes are generated in the perovskite layer and transported to respective electrodes through ETL and HTL. The dead (recombination) layer is shown in the inset.

Table 1

Parameters used in simulation of the perovskite solar cells. For better readability, parameters for holes and electrons are written in the brackets and without brackets, respectively.

	unit	ETL	perovskite	HTL
L	nm	40	375	45
N		20	60	20
ε_r		3.75	63	2.1
$\mu_{n(p)}$	$cm^2\,V^{-1}\,s^{-1}$	2×10^{-3}	24 (1)	(10^{-2})
$C_{n(p)}$	$10^{-14}\,m^3\,s^{-1}$	10^{-4}	5.56 (4.35)	(1)
N_t	m^{-3}	10^{22}	10^{21}	10^{22}
$\Gamma_{n(p)}$	$10^{-40}\,m^6\,s^{-1}$	4	1.55	(4)
ξ		10^{-4}	10^{-2}	10^{-4}
$E_{c(v)}$	eV	−4.0	−3.9 (−5.5)	(-5.35)
$N_{D(A)}$	m^{-3}	10^{20}	0 (0)	(1.4×10^{23})
$N_{c(v)}$	m^{-3}	2.5×10^{25}	8×10^{24}	(2.5×10^{25})

dominant in perovskite materials, it has been used for clarity in the simulation tool with symmetric values of $\Gamma_{n(p)}$ adopted from the literature [42]. Energy levels for the bottom of the conduction band (E_c) and the top of the valence band (E_v) for the $CH_3NH_3PbI_3$ are aligned to the energy band–gap equal to 1.6 eV acquired from UV–vis and PL measurements (see Fig. S3 (SI)) [43]. The injection barriers are associated with the Schottky contacts at the cathode/ETL and HTL/anode with the values equal to 0.1 eV and 0.15 eV, respectively. The ITO material represents the anode contact, whereas BCP/Au acts as the cathode contact. BCP is used as a tunneling transport layer which adjusts the energy level of gold to reduce the contact losses. Therefore, we could simulate these two layers as one with fixed energy alignment [44]. In the perovskite layer, there is assumed no doping ($N_{A(D)} = 0$). The values of the effective density of states $N_{c(v)}$ have been adopted from the literature [12]. The simulation properties of ETL and HTL have been chosen to resemble PCBM [12,45–48] and $CuNiO_x$ [49–52]: materials. The simulation temperature of the solar cells has been used the same as in the experiment (295 K). The built–in voltage equals to 1.13 V is similar to the values from the literature [12,30].

3. Results

The optical analysis performed with UV–vis and PL measurements is shown in Fig. S3 (SI). For the UV–vis experiment, the transmittance (T) and reflectance (R) of the samples have been measured and recalculated to the absorbance using a relation of 100% = A + T + R, the resulted absorbance is shown in Fig. S3a (SI). Using the tauc–plot, the optical band–gaps (E_g) have been obtained, which values were applied in the simulation. The E_g values of 1.601 eV, 1.595 eV and 1.591 eV were obtained for the thicknesses of 375 nm, 470 nm and 575 nm, respectively. The same shift of the band–gap is observed in PL measurements when the film thickness increases, see Fig. S3b (SI). The possible explanation of the effect is in–plane tensile strain perpendicular to the substrate which increases with film thickness and may impact the band–gap [53].

In order to characterize a crystal structure of the perovskite layer, the XRD measurements have been performed. Fig. S4a (SI) illustrates the XRD results of the perovskite which show negligible differences for three different thicknesses. The samples exhibit tetragonal phase with *I4cm* symmetry, which is confirmed by the diffraction peak with highest intensity of (110) [54]. Most importantly, in all three samples, we can see a very small diffraction peak observed at about 13° related to a secondary PbI_2 phase. The morphology of $CH_3NH_3PbI_3$ material is analyzed on the glass substrate with AFM measurements, see Figs. S3b–d in SI. The layers exhibit a very good coverage with the large grains of approximately 215 nm, 226 nm and 239 nm (statistics done on about 150 grains) for 375 nm, 470 nm and 575 nm thick layers, respectively.

The PSCs have been measured under AM1.5 conditions. Fig. 2 shows

the results for the PSCs with the perovskite thickness of 375 nm for two structures with $Cu:NiO_x$ and $Cu:NiO_x/PTAA$. It has been observed that the samples without PTAA material have PCE lower by about 2–3% (Fig. 2a). This behavior is mostly due to 1 mA cm^{-2} losses of J_{sc} and 100 mV of V_{oc}, see Fig. 2b,d, while FF remains the same for both types of devices (Fig. 2c). The same effect could be observed for the samples with thicker absorber layer (470 nm and 575 nm), as seen in Figs. S5–S6 (SI). However, the losses of V_{oc} and J_{sc} increase with increasing the thickness of perovskite absorber. For the samples with perovskite thickness of 575 nm, the V_{oc} and J_{sc} drops are about 200 mV and 2 mA cm^{-2}, respectively, which results in approximately 4% of PCE losses. The PSCs with modified HTL maintain high PCE with slight increase in efficiency when the perovskite layer thickness increases. This originates mostly due to higher J_{sc} which rises with the increasing the absorber thickness due to higher absorption of light in the red part of the spectrum [55]. It is also shown that using only PTAA thin film as HTL the perovskite solar cell works similar to structure with $Cu:NiO_x/PTAA$, see Fig. S7 (SI). For all analyzed types of devices, the FF slightly decreases with higher layer thickness. This is most probably related to increase of bulk recombination for thicker perovskite layers [56]. The observed parasitic phenomenon is likely related to surface recombination at HTL/$CH_3NH_3PbI_3$ interface as the only $Cu:NiO_x$ has been modified. Such an effect has been already reported for perovskite solar cells [12]. However, for a high surface recombination, it is expected that FF also should be affected. In this study, we further demonstrate that the concept of a dead layer with a very high trap recombination is able to explain the losses in photocurrent and voltage with small impact on FF.

The representative J–V curves and EQE of the two types of devices with the perovskite absorber thickness of 375 nm is shown in Fig. 3. For both cells, we can see the hysteresis effect is relatively small, which suggests a good quality of the perovskite layer, see Table 2. This is very important for further simulation analysis, because it has been reported that the hysteresis is smaller for p–i–n structure which should be related to the interface defects that influence different rates of ion migration [8,57]. Therefore, in the simulated device configuration we can neglect the impact of ions. The result of maximum power tracking (MPPT) shows good light stability of the cells during 150 s of measurements under AM1.5 light spectrum (Fig. 3a-inset). Fig. 3b illustrates the External Quantum Efficiency (EQE) for the same perovskite solar cells. It is observed that the total photocurrent of each cell calculated from EQE also proves the losses of 1 mA cm^{-2} (J_{sc}).

The experimental J–V characteristics have been used for the simulation process with the parameters given in Table 1. The profile of charge carriers generation (G) has been calculated with the transfer matrix model [58,59] which uses an extinction coefficient (κ) and a refractive index (η) in a function of wavelength, see Fig. S1 (SI). The obtained carriers generation profiles for both PSC structures with $Cu:NiO_x$ and $Cu:NiO_x/PTAA$ are presented in Fig. S8 (SI). It should be mentioned that there is no charge carriers generation within a recombination layer [18]. Validation of the simulation model, which is in an excellent agreement with the experimental results is shown in Fig. 4 for both PSCs structures. The detailed simulations for both structures at the illumination of 1 sun are presented in Figs. S9–S10 (SI). Fig. S9 (SI) demonstrates that at short–circuit conditions the presence of a dead layer only slightly influences a charge carriers concentration (part a), an electric field distribution (part b), and an energy alignment (part c). However, in Fig. S9d (SI) there is visible loss of electron and hole photocurrent due to the presence of the dead layer. At the open–circuit voltage (V_{oc}), we can see that high recombination in the dead layer drastically impacts on the charge carriers distribution not only at the interface but also in the bulk (Fig. S11a (SI)). Therefore, we will further focus only on V_{oc} conditions. As a result of the shift in charge carrier densities, the electric field distribution has changed throughout the sample. It is due to a higher value of $|E|$ at the interfaces between perovskite/ETL and HTL/perovskite. The effect of a dead layer also slightly influences the alignment of conduction and valence bands. However, the
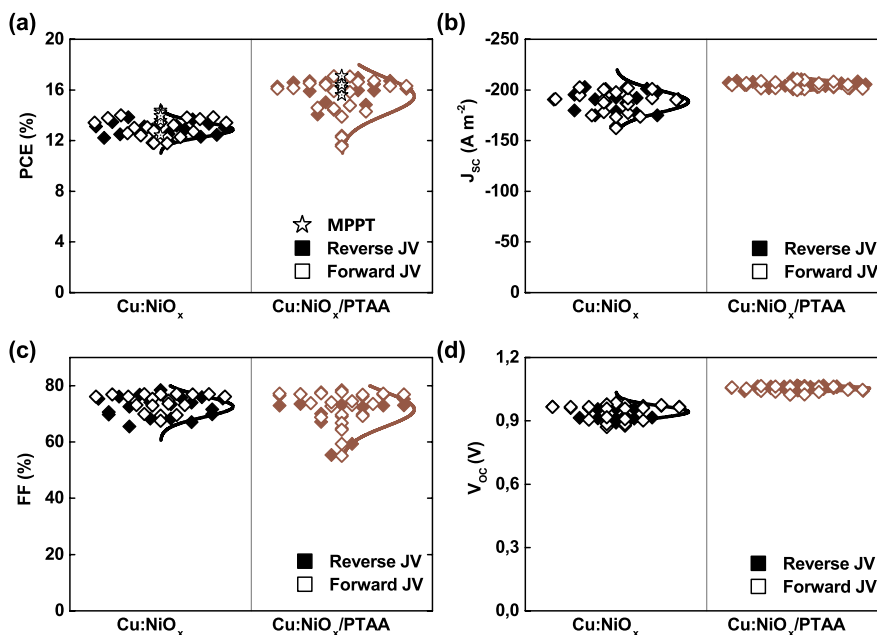
Fig. 2. Photovoltaic parameters for PSCs, a) PCE, b) J_{sc}, c) FF, and d) V_{oc}. Solar cell structure with Cu:NiO$_x$ (black symbols) and Cu:NiO$_x$/PTAA (red symbols) as HTL. Both stacks have 375 nm perovskite thickness.
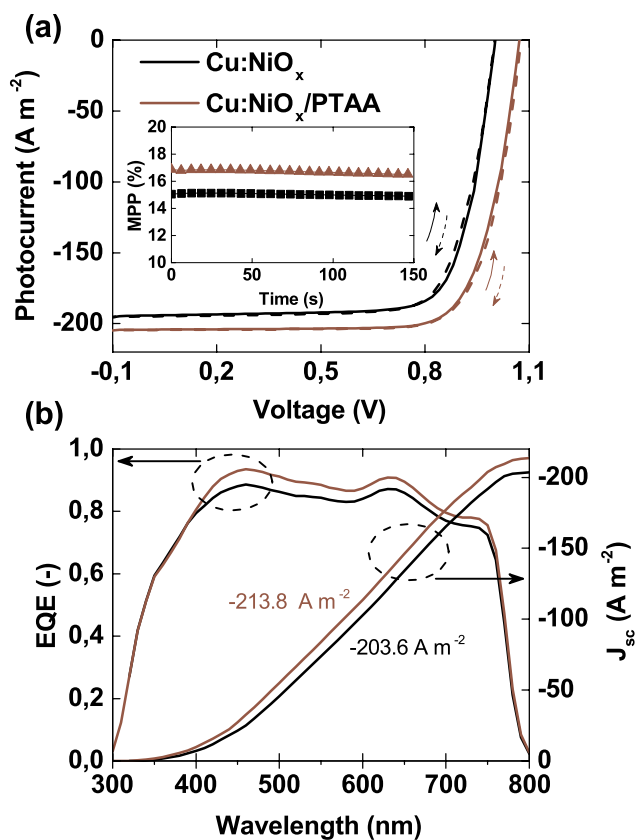

Fig. 3. The experimental results for two PSCs. a) J–V characteristics for forward (solid line) and reverse (dashed line) scans with the inset of MPPT for the cells. b) EQE and integrated photocurrent of the cells. The absorber thickness equals to 375 nm. Red and black lines represent Cu:NiO$_x$ with and without PTAA layer, respectively.
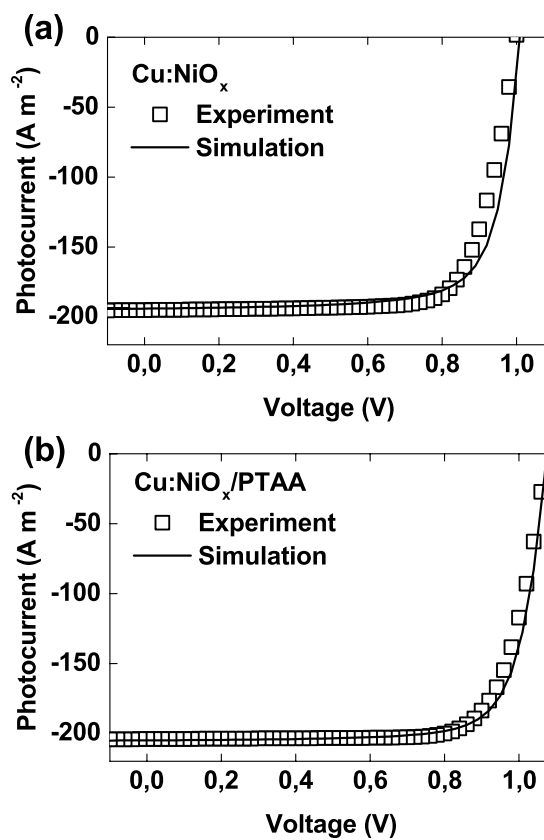
Fig. 4. Photocurrent–voltage characteristics for experimental (square symbol) and simulation (solid line) results for a) Cu:NiO$_x$ with 5 nm dead layer, and b) Cu:NiO$_x$/PTAA without dead layer. In the dead layer, the surface recombination velocities are equal to 3.75×10^3 and 3.75×10^4 m s^{-1} for electrons and holes, respectively. Other parameters used in simulations are the same for both devices and they are specified in Table 1.

Table 2
Photovoltaic parameters for the PSCs representative cells.

	Cu:NiO$_x$		Cu:NiO$_x$/PTAA	
	Forward	Reverse	Forward	Reverse
J_{sc} [A m^{-2}]	−194.24	−194.92	−204.25	−204.48
V_{oc} [V]	1.00	1.00	1.07	1.08
FF [%]	76.20	75.13	75.75	75.88
PCE [%]	14.84	14.66	16.58	16.71

most relevant impact of the dead layer is visible on the photocurrent distribution (Fig. S11d (SI)) which clearly shows the role of this recombination layer. It is observed that the electron and hole photocurrents reach the high values at HTL/perovskite interface, however, very high recombination in the dead layer leads to abrupt loss of the current. This effect is not visible in the sample without dead layer, as shown in Fig. S12d (SI). Also, it should be pointed out that the photocurrent distribution in the PSC with the dead layer is reversible in comparison to a sample without this layer. This will be later explained in more details.

It is well known that the same shape of a fitting curve could be obtained for different sets of parameters. However, simulation results are more precise when more physical variations are applied. Therefore, using light filters, the range of measurements has been extended for the representative samples. Fig. 5 shows the simulation results of the cell with Cu:NiO$_x$. These results are in excellent agreement with experimental results using the same set of parameters (Table 1) for a very wide range of the illumination profiles (0.001–1 suns). The numerical simulations with the use of either bulk or one dimensional surface recombination have not been able to explain all the observed experimental results. It should be also mentioned that only the chosen parameters could simultaneously explain all the variations including the surface passivation, the absorber thickness and the light intensity. Simulations have shown that the best fit for the dead (recombination) layer has been obtained if the thickness of dead layer is 5 nm and with the surface

recombination velocities equal to 3.75×10^3 and 3.75×10^4 m s^{-1} for electrons and holes, respectively. It is observed that holes recombine mostly in the dead layer. This effect originates from a location of the interface between the perovskite and HTL, where more holes are present. Fig. 5a shows the PCEs in respect to illumination. It should be noticed that the highest efficiency is reached at a light intensity of about 0.8 suns and starts to decrease for higher light intensities. The simulation results are in slight disagreement with the experiment at lower illuminations which are associated with almost dark conditions. The J_{sc} follows exactly the same trend for simulation and the experiment, which confirms a linear relationship between the current and light intensity in PSCs [60] and suggests that monomolecular recombination is dominant at a short–circuit [61] (Fig. 5b). The FF is the most sensitive photovoltaic parameter in simulation of solar cells. Even a slight change of any parameter in the numerical model may drastically change the final shape of the curve with different illumination intensities, see Fig. 5c. Also, the general shape of FF suggests a competition of two dominant recombinations in the PSCs. We can see that the FF decreases monotonically above 0.1 suns which is related to series resistance, bimolecular recombination or surface recombination. However, below 0.1 suns, the FF drops with a decreasing value of light intensity which should occur for a pure trap–assisted recombination [8]. Therefore, it is expected that charge carriers recombination is monomolecular for the low illumination. Also, a spread of the statistical bar at 0.001 suns should be related to the leakage current, which has a higher impact on FF at low intensities [62]. Fig. 5d shows the V_{oc} dependence from the light intensity. The calculated ideality factors (n_{id}) for the experimental and simulation results are very similar suggesting a good choice of dominant recombination channel. According to Tress et al. [63], the surface recombination dominates if the ideality factor is closer to 1, which is mainly observed for lower built–in voltage in a perovskite material. Therefore, the acquired value of $n_{id} \approx 1.4$ proves the idea of a high recombination at Cu:NiO$_x$/CH$_3$NH$_3$PbI$_3$ interface. The small flattening of V_{oc} at high intensities should be also related to high surface recombination in the dead layer.
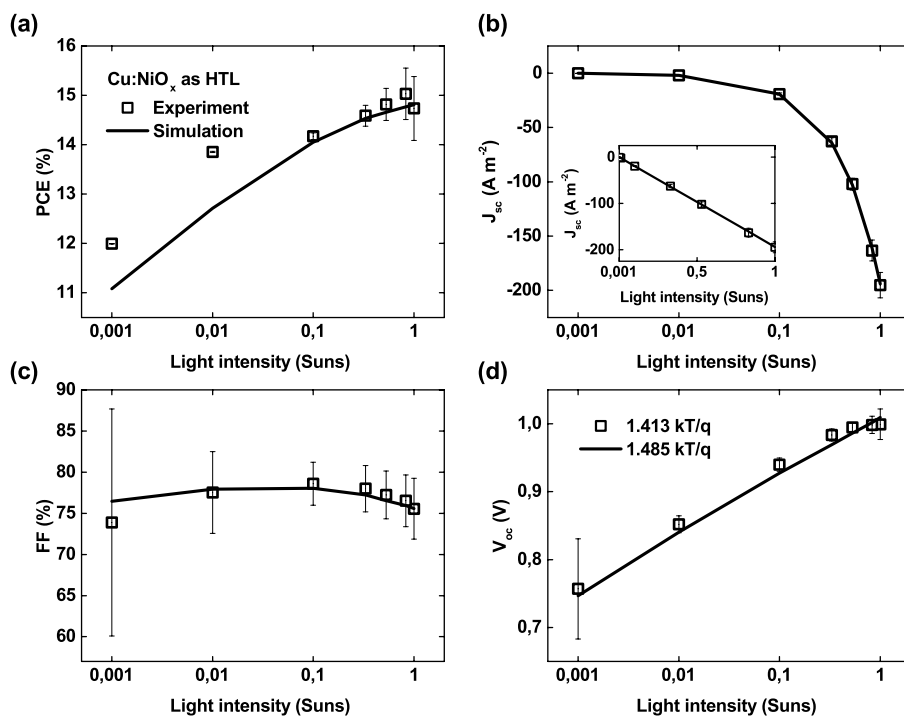

Fig. 5. Photovoltaic experimental (square symbol) and simulation (solid line) results for different illuminations. a) PCE, b) J$_{sc}$ with the inset presented the same result using linear scale of the light intensity, c) FF, and d) V$_{oc}$. Solar cell structure with Cu:NiO$_x$ as HTL. Parameters are the same as used in Fig. 4a. 1 sun = 100 mW cm^{-2}.

Fig. 6 shows photovoltaic parameters as a function of light intensity for Cu:NiO$_x$/PTAA in the perovskite solar cell. The passivation with PTAA is assumed to reduce the surface recombination. Therefore in the simulation, we have used the same set of parameters but with a removed dead layer. The simulated and experimental results show a very good agreement, which finally proves the existence of the dead layer at Cu:NiO$_x$. It appears to be the simplest way to improve the interface and remove the parasitic recombination. The PCE results for different illuminations are similar to the previous ones, however, lowered by about 2%, see Fig. 6a. Fig. 6b-inset presents a linear trend of J$_{sc}$ as a function of light intensity. It suggests monomolecular recombination as a dominant mechanism in this region. The FF in respect to the light intensity shows very similar behavior as the PSC with the dead layer, as seen in Fig. 6c. However, there is no surface recombination in this system. Therefore the region above 0.1 suns, where FF starts to increase, should be associated with bimolecular recombination. At low illumination, a monomolecular recombination still dominates. In Fig. 6d, n$_{id}$ is approximately 1.7 at the open–circuit voltage. A value of the ideality factor closer to 2 confirms the existence of the trap–assisted SRH recombination as a dominant recombination channel in the bulk.

Fig. 7 illustrates the simulation results for the PSC at different illumination intensities. The results are presented only for the current distribution which is a representative variable for the analysis of a dead recombination layer. It should be mentioned that the total current in each simulation is always about zero, because the open–circuit condition is used in the simulation. However, the amplitude of current within the simulated sample decreases proportionally with decreasing the light intensity. Fig. 7a shows the PSC simulated at 1 sun illumination. It has been already noticed that the current distribution is reversed at the interface of the dead layer (Figs. S11–S12 (SI)). However, the current distribution gets back to the normal distribution at the HTL interface for lower light intensity, see Fig. 7b and c. The explanation of this effect is related to high asymmetric recombination in the dead layer. If light intensity increases, the total charge carrier concentration has a higher value. Therefore, the dominant recombination should be proportionally higher in the parasitic layer. As the surface recombination is

asymmetric, it leads to inversion of a total distribution of photocurrent. However, at very low light intensities, where almost dark conditions are observed, the charge carrier density is much lower. Thus, the surface recombination is not strongly influencing the shape of the photocurrent distribution. As a consequence, it starts to resemble the sample without a dead layer, see Fig. 7d and Fig. S13d (SI).

Further, the influence of dead layer thickness and a surface recombination velocity with illumination intensities were analyzed. Fig. 8 shows photovoltaic parameters for the PSCs with 2 nm, 5 nm (as a reference) and 10 nm dead layer with a constant surface recombination velocity. Fig. 8a demonstrates that the PCE is decreasing with increasing the thickness of the recombination layer. This trend is especially visible at high illumination intensities. The efficiency decreases mostly due to the loss of short–circuit photocurrent, see Fig. 8b. This occurs due to the fact that no charge carriers are generated within the recombination layer and even small losses in the generation profile from an illumination side influence the total photocurrent. Fig. 8c illustrates the resulted FF. It should be noticed that the thicker the parasitic layer is, the more visible is a monotonic rise of the FF above 0.1 suns. This effect originates from the higher domination of the surface recombination. Recently, it has been reported that the fill–factor monotonically decreases in the whole range of illumination when the surface recombination is the only recombination mechanism [12]. From V$_{oc}$ analysis, it is clear that the ideality factor gets closer to 1 for a higher thickness of the recombination layer, as shown in Fig. 8d. The same trends were obtained for the different surface recombination velocities with a constant thickness of the dead layer, Fig. S14 (SI). The reason is that the recombination rate depends both on the thickness and the surface recombination velocity. Therefore, the same rate could be acquired with different parameters. However, a thickness of the dead layer also influences the photocurrent in contrast to a surface recombination velocity, which finally confirms our choice of recombination mechanisms (Fig. S14b-inset (SI)).

Fig. 9 shows spatial dependencies for different dead layer thicknesses. For clarity, the distributions are only presented for the absorber layer. It is observed that, for the higher surface recombination rates, the smaller values of a total charge carriers density within the absorber were
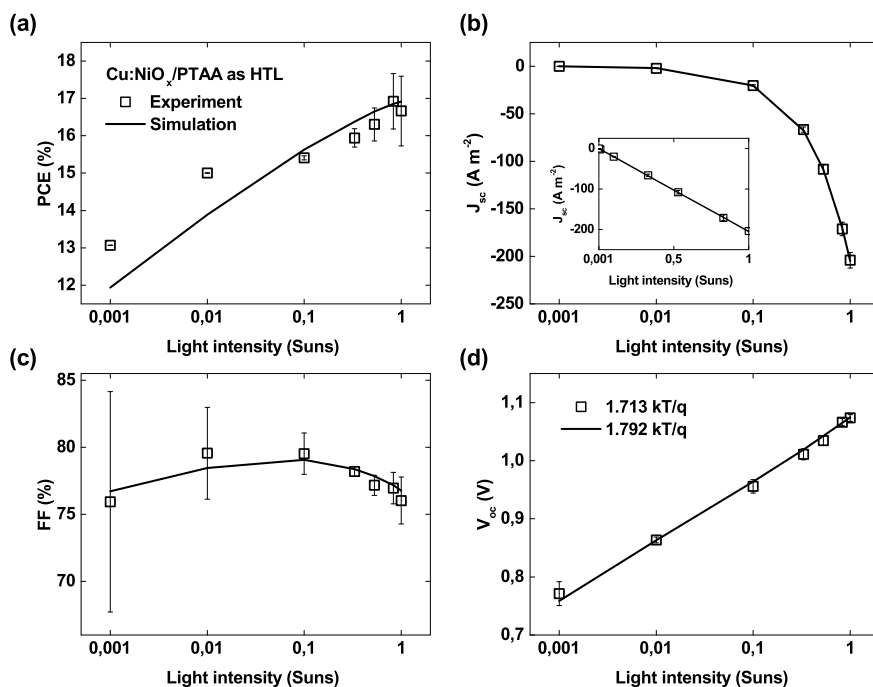

Fig. 6. Photovoltaic experimental (square symbol) and simulation (solid line) results for different illuminations. a) PCE, b) J$_{sc}$ with the inset presented the same result using linear scale of the light intensity, c) FF, and d) V$_{oc}$. Solar cell structure with Cu:NiO$_x$/PTAA as HTL. Parameters are the same as used in Fig. 4b. 1 sun = 100 mW cm^{-2}.
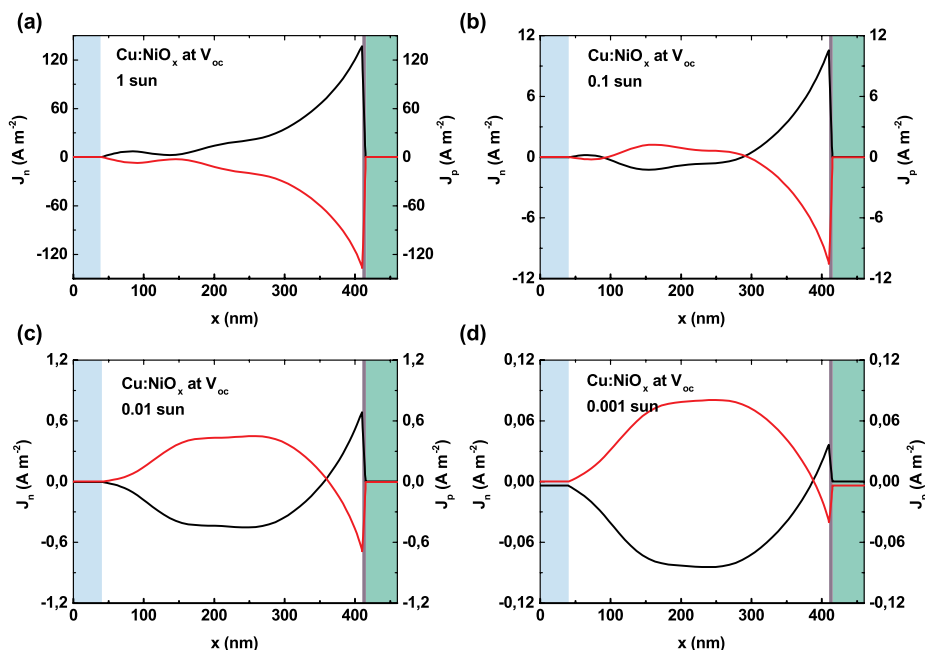
Fig. 7. Spatial distributions of electron (black line) and hole (red line) photocurrents calculated for an open–circuit voltage (V_{oc}) at illumination equal to a) 1 sun, b) 0.1 sun, c) 0.01 sun, and c) 0.001 sun. All simulations are done for solar cell structure with dead layer (violet area) at the interface, and also with PCBM (blue area) and the perovskite (white area). All the parameters are the same as used in Fig. 4a.

obtained, see Fig. 9a. The difference between electron and hole concentrations rises with increasing the thickness of the dead layer. This leads to the fact that the electric field increases linearly, see Fig. 9b. However, these changes in the concentrations and the electric field impact the diffusion and drift currents. Therefore, the total photocurrent is also varying with different recombination layer thicknesses, see Fig. 9c. The average current approaches zero for the open–circuit conditions, however the amplitude increases with increasing a thickness of the dead layer. Fig. S15 (SI) presents the same behavior for different surface recombination velocities. It shows that the presence of parasitic dead layer in the PSCs has a significant effect on the working operation even with its relatively small thickness and twice smaller surface recombination velocity.

4. Experimental section

4.1. Device fabrication

The precursor for perovskite $CH_3NH_3PbI_3$ phase was prepared as described below. Commercial lead iodide (PbI_2) (99.99%, TCI), methylammonium iodide (MAI) (GreatCell Solar), dimethylformamide (DMF) solvent (99.8%, Sigma-Aldrich) and 1-methyl-2-pyrrolidinone (NMP) solvent (99.5%, ACROS Organics), were used as received. The powders of MAI and PbI_2 were mixed in 1:1 molar ratio and dissolved in DMF:NMP (9:1 vol ratio) solution by stirring overnight at room temperature. Three precursors solutions with 1 M, 1.2 M and 1.4 M equimolar concentrations were used in all experimental section. Patterned glass/ITO substrates were ultrasonically cleaned with soap water, deionized water, and ethanol, followed UV–ozone treatment for 30 min. All the solar cells preparation processes were carried out inside the nitrogen–filled glove–box with oxygen and moisture levels about 1 ppm. The HTL of $Cu:NiO_x$ was prepared from 0.95 mmol $Ni(NO_3)_2 \cdot 6\,H_2O$ and 0.05 mmol $Cu(NO_3)_2 \cdot 3\,H_2O$ powders mixed in 9:1 volumetric ratio of 2-methoxyethanol solution and acetyloaceton solutions, respectively. The $Cu:NiO_x$ was spin–coated at 1500 RPM for 60 s with acceleration 1500 RPM s^{-1}. It was dried on hot–plate for 5 min at 150°C in N_2 environment, and further for 15 min at 300°C in air. The surface passivation of $Cu:NiO_x$ has been done with poly(triaryl amine) (PTAA) (Sigma-Aldrich) solution

in toluene with the concentration of $2\,mg\,mL^{-1}$. The solution was spin–coated at 5000 RPM for 35 s with the acceleration of 5000 RPM s^{-1}. Then samples were annealed at 100°C in N_2 for 10 min. Subsequently, the perovskite solution was dynamically spin–coated with the following gas quenching [64]. The 100 μL precursor was spin–coated on glass substrate in two steps. First, at 2000 RPM for 10 s with acceleration 200 RPM s^{-1} and, then at 5000 RPM for 30 s with 2000 RPM s^{-1}. After 15 s of spin–coating, the N_2 gun was used for quenching the perovskite layer for 15 s at 6 bars pressure with 10 cm vertical position from the substrate. Afterwards, the samples were immediately placed on the hot–plate at 100°C for 10 min. The ETL solution was prepared by dissolving $20\,mg\,mL^{-1}$ of [6,6]-phenyl C61 butyric acid methyl ester (PCBM) (99%, Solenne) in chlorobenzene, the solution which was stirred overnight at 60°C. ETL was spin-coated at 1500 RPM for 55 s with the acceleration of 3000 RPM s^{-1} and followed by spin–coating of bathocuproine (BCP) (99.99%, Sigma-Aldrich) solution of $0.5\,mg\,mL^{-1}$ in ethanol at 3000 RPM for 50 s with the acceleration of 3000 RPM s^{-1}. Subsequently, the cleaning of ITO contacts from HTL, the perovskite and ETL layers was done in air with the use of DMF:chlorobenzene solution in 1:6 vol ratio. Finally, Au electrodes were thermally deposited with a thickness of 100 nm under the pressure of 1×10^{-6} mbar through a shadow mask on top of the ETLs.

4.2. Characterization

The film thickness of each layer was measured with Bruker XT Dektak profilometer giving for the $CH_3NH_3PbI_3$ perovskite material 375 ± 5 nm, 470 ± 2 nm and 575 ± 4 nm for 1 M, 1.2 M and 1.4 M molar concentrations, respectively. The crystal structure characterization was performed using a Bragg–Brentano geometry X–ray diffractometer (PanAlytical Empyrean; referred as XRD). The morphology was investigated with atomic force microscope (Park NX-10 tool; referred as AFM). The optical properties of the samples were measured with UV–vis spectrophotometer (Agilent Cary 5000) by measuring the transmittance (T) and the reflectance (R). Steady–state photoluminescence spectrum (Horiba Labram Aramis system; referred as PL) was measured with an excitation laser beam at 532 nm and Si detector. The current–voltage (J–V) characteristics of solar cells were measured in N_2 filled glove–box
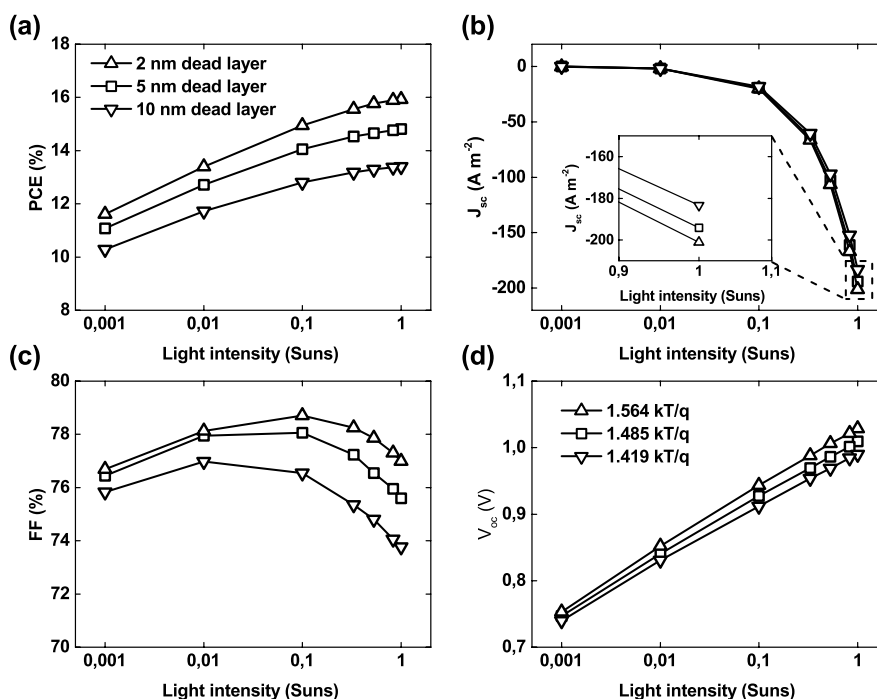
Fig. 8. Photovoltaic parameters for different illuminations. a) PCE, b) J_{sc} with inset presented results at 1 sun, c) FF, and d) V_{oc}. Solar cell structure includes dead layer with 2 nm (triangle up symbol), 5 nm (square symbol) and 10 nm (triangle down symbol) thicknesses. Surface recombination velocities equal to 3.75×10^3 and 3.75×10^4 m s^{-1} for electrons and holes, respectively. 1 sun = 100 mW cm^{-2}.

under a white light halogen lamp using illumination mask of 0.09 cm^2, to define the active area of the sample. The light intensity was calibrated to 100 mW cm^{-2} with a silicon reference cell to simulate AM1.5 spectrum. However, for obtaining different illuminations, the set of neutral filters have been used to obtain 1, 0.83, 0.53, 0.33, 0.1, 0.01 and 0.001 sun intensities. The J–V curves were measured with Keithley 2400 with a scanning rate of 0.165 V s^{-1} with 20 mV step. The scanning was performed in forward (from −0.1 V to 1.1 V) and reverse (from 1.1 V to −0.1 V) bias to show the effect of hysteresis. The measurements of J–V characteristics were done without preconditioning with light soaking or UV treatment. The maximum power point tracking (MPPT) was performed for approximately 2 min with continuous illumination, and control of voltage and current at maximum power point. The external quantum efficiency (EQE) was measured with setup from Rera Solutions.

5. Summary

Two types of perovskite solar cells with different HTLs (Cu:NiO$_x$ and Cu:NiO$_x$/PTAA) were analyzed. The experimental results demonstrate that significant recombination losses are observed in the PV devices without PTAA material. It leads to a photocurrent and voltage drop of 1–2 mA cm^{-2} and 100–200 mV, respectively. This in turn leads to the loss of efficiency by 2–4%, which values are perovskite thickness dependent. The simulations based on the drift–diffusion model have shown the presence of a dead (recombination) layer at the interface of HTL/perovskite in the solar cell with Cu:NiO$_x$ as HTL. The thickness of this recombination layer is estimated to be 5 nm for a 375 nm thick layer of the perovskite absorber. Results of spatial simulations have confirmed that the dead layer influences the charge carrier density and the electric field distribution. However, the most visible impact is observed on the current distribution within the solar cell. The same parasitic recombination phenomenon could be observed in any PSCs with p–i–n configuration, where metal oxides would be used as HTL. Therefore, the performed analysis could help to further improve the performance and give a better understanding of the recombination mechanisms in perovskite solar cells.
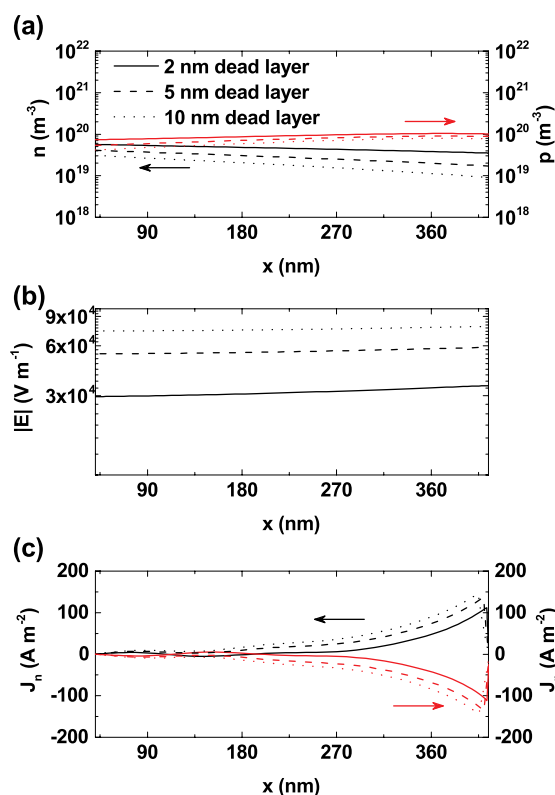

Fig. 9. Spatial simulation results for an open–circuit voltage (V_{oc}) at 1 sun illumination only for the perovskite layer. a) Electron (black line) and hole (red line) density distributions, b) absolute electric field distribution, and c) electron (black line) and hole (red line) photocurrents. The simulation distance is in respect to cathode (Au) electrode. The parameters used are the same as in Fig. 8.

Declaration of interests

The authors declare that they have no known competing financial interests or personal relationships that could have appeared to influence the work reported in this paper.

Appendix A. Supplementary data

Supplementary data to this article can be found online at https://doi.org/10.1016/j.nanoen.2019.104186.

References

[1] National Renewable Energy Laboratory (NREL), Chart of best research-cell efficiencies. https://www.nrel.gov/pv/assets/images/efficiency-chart.png, 2, 22, 2019.

[2] L.M. Herz, Charge-carrier dynamics in organic-inorganic metal halide perovskites, Annu. Rev. Phys. Chem. 67 (1) (2016) 65–89.

[3] T. Leijtens, S.D. Stranks, G.E. Eperon, R. Lindblad, E.M.J. Johansson, I.J. McPherson, H. Rensmo, J.M. Ball, M.M. Lee, H.J. Snaith, Electronic properties of meso-superstructured and planar organometal halide perovskite films: charge trapping, photodoping, and carrier mobility, ACS Nano 8 (7) (2014) 7147–7155.

[4] A. Miyata, A. Mitioglu, P. Plochocka, O. Portugall, J.T.-W. Wang, S.D. Stranks, H.J. Snaith, R.J. Nicholas, Direct measurement of the exciton binding energy and effective masses for charge carriers in organic-inorganic tri-halide perovskites, Nat. Phys. 11 (7) (2015) 582–587.

[5] Y.M. Wang, S. Bai, L. Cheng, N.N. Wang, J.P. Wang, F. Gao, W. Huang, High-efficiency flexible solar cells based on organometal halide perovskites, Adv. Mater. 28 (22) (2016) 4532–4540.

[6] W.E.I. Sha, X. Ren, L. Chen, W.C.H. Choy, The efficiency limit of $CH_3NH_3PbI_3$ perovskite solar cells, Appl. Phys. Lett. 106 (22) (2015) 221104.

[7] D. Yang, R. Yang, K. Wang, C. Wu, X. Zhu, J. Feng, X. Ren, G. Fang, S. Priya, S.F. Liu, High efficiency planar-type perovskite solar cells with negligible hysteresis using EDTA-complexed $_s$, Nat. Commun. 9 (1) (2018) 3239.

[8] T.S. Sherkar, C. Momblona, L. Gil-Escrig, J. Ávila, M. Sessolo, H.J. Bolink, L.J.A. Koster, Recombination in perovskite solar cells: significance of grain boundaries, interface traps, and defect ions, ACS Energy Lett 2 (5) (2017) 1214–1222.

[9] G.-J.A.H. Wetzelaer, M. Scheepers, A.M. Sempere, C. Momblona, J. Ávila, H.J. Bolink, Trap-assisted non-radiative recombination in organic–inorganic perovskite solar cells, Adv. Mater. 27 (11) (2015) 1837–1841.

[10] Y. Shao, Y. Fang, T. Li, Q. Wang, Q. Dong, Y. Deng, Y. Yuan, H. Wei, M. Wang, A. Gruverman, J. Shield, J. Huang, Grain boundary dominated ion migration in polycrystalline organic–inorganic halide perovskite films, Energy Environ. Sci. 9 (2016) 1752–1759.

[11] X. Wu, M.T. Trinh, D. Niesner, H. Zhu, Z. Norman, J.S. Owen, O. Yaffe, B.J. Kudisch, X.-Y. Zhu, Trap states in lead iodide perovskites, J. Am. Chem. Soc. 137 (5) (2015) 2089–2096.

[12] T.S. Sherkar, C. Momblona, L. Gil-Escrig, H.J. Bolink, L.J.A. Koster, Improving perovskite solar cells: insights from a validated device model, Adv. Energy Mater. 7 (13) (2017) 1602432.

[13] A.B. Sproul, Dimensionless solution of the equation describing the effect of surface recombination on carrier decay in semiconductors, J. Appl. Phys. 76 (5) (1994) 2851–2854.

[14] N.J. Halas, J. Bokor, Surface recombination on the Si(111) 2×1 surface, Phys. Rev. Lett. 62 (1989) 1679–1682.

[15] X. Wen, W. Chen, J. Yang, Q. Ou, T. Yang, C. Zhou, H. Lin, Z. Wang, Y. Zhang, G. Conibeer, Q. Bao, B. Jia, D.J. Moss, Role of surface recombination in halide perovskite nanoplatelets, ACS Appl. Mater. Interfaces 10 (37) (2018) 31586–31593.

[16] J. Wang, W. Fu, S. Jariwala, I. Sinha, A.K.-Y. Jen, D.S. Ginger, Reducing surface recombination velocities at the electrical contacts will improve perovskite photovoltaics, ACS Energy Lett 4 (1) (2019) 222–227.

[17] J. Idígoras, L. Contreras-Bernal, J.M. Cave, N.E. Courtier, A. Barranco, A. Borras, J.R. Sánchez-Valencia, J.A. Anta, A.B. Walker, The role of surface recombination on the performance of perovskite solar cells: effect of morphology and crystalline phase of TiO2 contact, Adv. Mater. Interfaces 5 (21) (2018) 1801076.

[18] A. Nakane, H. Tampo, M. Tamakoshi, S. Fujimoto, K.M. Kim, S. Kim, H. Shibata, S. Niki, H. Fujiwara, Quantitative determination of optical and recombination losses in thin-film photovoltaic devices based on external quantum efficiency analysis, J. Appl. Phys. 120 (6) (2016), 064505.

[19] C.J. Flynn, S.M. McCullough, L. Li, C.L. Donley, Y. Kanai, J.F. Cahoon, Passivation of nickel vacancy defects in nickel oxide solar cells by targeted atomic deposition of boron, J. Phys. Chem. C 120 (30) (2016) 16568–16576.

[20] S. Olthof, K. Meerholz, Substrate-dependent electronic structure and film formation of MAPbI3 perovskites, Sci. Rep. 7 (2017) 40267.

[21] Y. Cheng, M. Li, X. Liu, S.H. Cheung, H.T. Chandran, H.-W. Li, X. Xu, Y.-M. Xie, S.K. So, H.-L. Yip, S.-W. Tsang, Impact of surface dipole in niox on the crystallization and photovoltaic performance of organometal halide perovskite solar cells, Nano Energy 61 (2019) 496–504.

[22] P. Cui, P. Fu, D. Wei, M. Li, D. Song, X. Yue, Y. Li, Z. Zhang, Y. Li, J.M. Mbengue, Reduced surface defects of organometallic perovskite by thermal annealing for highly efficient perovskite solar cells, RSC Adv. 5 (2015) 75622–75629.

[23] H. Zhu, B. Huang, S. Wu, Z. Xiong, J. Li, W. Chen, Facile surface modification of $CH_3NH_3PbI_3$ films leading to simultaneously improved efficiency and stability of inverted perovskite solar cells, J. Mater. Chem. A 6 (2018) 6255–6264.

[24] X. He, Y. Bai, H. Chen, X. Zheng, S. Yang, High performance perovskite solar cells through surface modification, mixed solvent engineering and nanobowl-assisted light harvesting, MRS Adv. 1 (47) (2016) 3175–3184.

[25] E.Y. Tiguntseva, I.N. Saraeva, S.I. Kudryashov, E.V. Ushakova, F.E. Komissarenko, A.R. Ishteev, A.N. Tsypkin, R. Haroldson, V.A. Milichko, D.A. Zuev, S.V. Makarov, A.A. Zakhidov, Laser post-processing of halide perovskites for enhanced photoluminescence and absorbance, J. Phys. Conf. Ser. 917 (6) (2017), 062002.

[26] D. Głowienka, J. Szmytkowski, Numerical modeling of exciton impact in two crystallographic phases of the organo-lead halide perovskite ($CH_3NH_3PbI_3$) solar cell, Semicond. Sci. Technol. 34 (3) (2019), 035018.

[27] P. Calado, A.M. Telford, D. Bryant, X. Li, J. Nelson, B.C. O'Regan, P.R.F. Barnes, Evidence for ion migration in hybrid perovskite solar cells with minimal hysteresis, Nat. Commun. 7 (2016) 13831.

[28] S. Van Reenen, M. Kemerink, H.J. Snaith, Modeling anomalous hysteresis in perovskite solar cells, J. Phys. Chem. Lett. 6 (19) (2015) 3808–3814.

[29] X. Ren, Z. Wang, W.E. Sha, W.C. Choy, Exploring the way to approach the efficiency limit of perovskite solar cells by drift-diffusion model, ACS Photonics 4 (4) (2017) 934–942.

[30] G. Richardson, S. O'Kane, R.G. Niemann, T. Peltola, J.M. Foster, P.J. Cameron, A. Walker, Can slow-moving ions explain hysteresis in the current-voltage curves of perovskite solar cells? Energy Environ. Sci. 9 (2016) 1476–1485.

[31] Y. Zhou, A. Gray-Weale, A numerical model for charge transport and energy convention of perovskite solar cells, Phys. Chem. Chem. Phys. 18 (2015) 4476–4486.

[32] D. Walter, A. Fell, Y. Wu, T. Duong, C. Barugkin, N. Wu, T. White, K. Weber, Transient photovoltage in perovskite solar cells: interaction of trap-mediated recombination and migration of multiple ionic species, J. Phys. Chem. C 122 (21) (2018) 11270–11281.

[33] Z.S. Wang, W.E.I. Sha, W.C.H. Choy, Exciton delocalization incorporated drift-diffusion model for bulk-heterojunction organic solar cells, J. Appl. Phys. 120 (21) (2016) 213101.

[34] M. Lundstrom, R. Schuelke, Modeling semiconductor heterojunctions in equilibrium, Solid State Electron. 25 (8) (1982) 683–691.

[35] M.S. Lundstrom, R.J. Schuelke, Numerical analysis of heterostructure semiconductor devices, IEEE Trans. Electron Dev. 30 (9) (1983) 1151–1159.

[36] M. Gruber, B. Stickler, G. Trimmel, F. Schurrer, K. Zojer, Impact of energy alignment and morphology on the efficiency in inorganic–organic hybrid solar cells, Org. Electron. 11 (12) (2010) 1999–2011.

[37] Q. Lin, A. Armin, R.C.R. Nagiri, P.L. Burn, P. Meredith, Electro-optics of perovskite solar cells, Nat. Photonics 9 (2) (2015) 106–112.

[38] N. Onoda-Yamamuro, T. Matsuo, H. Suga, Dielectric study of $CH_3NH_3PbX_3$ ($X = Cl$, Br, I), J. Phys. Chem. Solids 53 (7) (1992) 935–939.

[39] B. Maynard, Q. Long, E.A. Schiff, M. Yang, K. Zhu, R. Kottokkaran, H. Abbas, V.L. Dalal, Electron and hole drift mobility measurements on methylammonium lead iodide perovskite solar cells, Appl. Phys. Lett. 108 (17) (2016) 173505.

[40] D. Kiermasch, P. Rieder, K. Tvingstedt, A. Baumann, V. Dyakonov, Improved charge carrier lifetime in planar perovskite solar cells by bromine doping, Sci. Rep. 6 (2016) 1–7.

[41] J.G. Simmons, G.W. Taylor, Nonequilibrium steady-state statistics and associated effects for insulators and semiconductors containing an arbitrary distribution of traps, Phys. Rev. B 4 (1971) 502–511.

[42] R.L. Milot, G.E. Eperon, H.J. Snaith, M.B. Johnston, L.M. Herz, Temperature-dependent charge-carrier dynamics in $CH_3NH_3PbI_3$ perovskite thin films, Adv. Funct. Mater. 25 (39) (2015) 6218–6227.

[43] X. Sun, C. Zhang, J. Chang, H. Yang, H. Xi, G. Lu, D. Chen, Z. Lin, X. Lu, J. Zhang, Y. Hao, Mixed-solvent-vapor annealing of perovskite for photovoltaic device efficiency enhancement, Nano Energy 28 (2016) 417–425.

[44] T. Sakurai, S. Wang, S. Toyoshima, K. Akimoto, Role of electrode buffer layers in organic solar cells, in: 2013 International Renewable and Sustainable Energy Conference (IRSEC), IEEE, 2013, pp. 46–48.

[45] G. Garcia-Belmonte, A. Munar, E.M. Barea, J. Bisquert, I. Ugarte, R. Pacios, Charge carrier mobility and lifetime of organic bulk heterojunctions analyzed by impedance spectroscopy, Org. Electron. 9 (5) (2008) 847–851.

[46] R.C.I. MacKenzie, T. Kirchartz, G.F.A. Dibb, J. Nelson, Modeling nongeminate recombination in P3HT:PCBM solar cells, J. Phys. Chem. C 115 (19) (2011) 9806–9813.

[47] D.B. Khadka, Y. Shirai, M. Yanagida, J.W. Ryan, K. Miyano, Exploring the effects of interfacial carrier transport layers on device performance and optoelectronic properties of planar perovskite solar cells, J. Mater. Chem. C 5 (2017) 8819–8827.

[48] G. Juška, K. Genevičius, N. Nekrašas, G. Sliaužys, G. Dennler, Trimolecular recombination in polythiophene: fullerene bulk heterojunction solar cells, Appl. Phys. Lett. 93 (14) (2008) 143303.

[49] K. Yao, F. Li, Q. He, X. Wang, Y. Jiang, H. Huang, A.K.-Y. Jen, A copper-doped nickel oxide bilayer for enhancing efficiency and stability of hysteresis-free inverted mesoporous perovskite solar cells, Nano Energy 40 (2017) 155–162.

[50] S. Yue, K. Liu, R. Xu, M. Li, M. Azam, K. Ren, J. Liu, Y. Sun, Z. Wang, D. Cao, X. Yan, S. Qu, Y. Lei, Z. Wang, Efficacious engineering on charge extraction for realizing highly efficient perovskite solar cells, Energy Environ. Sci. 10 (2017) 2570–2578.

[51] G. Natu, P. Hasin, Z. Huang, Z. Ji, M. He, Y. Wu, Valence band-edge engineering of nickel oxide nanoparticles via cobalt doping for application in p-type dye-sensitized solar cells, ACS Appl. Mater. Interfaces 4 (11) (2012) 5922–5929.

[52] Q. He, K. Yao, X. Wang, X. Xia, S. Leng, F. Li, Room-temperature and solution-processable Cu-doped nickel oxide nanoparticles for efficient hole-transport layers of flexible large-area perovskite solar cells, ACS Appl. Mater. Interfaces 9 (48) (2017) 41887–41897.

[53] C. Zhu, X. Niu, Y. Fu, N. Li, C. Hu, Y. Chen, X. He, G. Na, P. Liu, H. Zai, Y. Ge, Y. Lu, X. Ke, Y. Bai, S. Yang, P. Chen, Y. Li, M. Sui, L. Zhang, H. Zhou, Q. Chen, Strain engineering in perovskite solar cells and its impacts on carrier dynamics, Nat. Commun. 10 (1) (2019) 815.

[54] D. Głowienka, T. Miruszewski, J. Szmytkowski, The domination of ionic conductivity in tetragonal phase of the organometal halide perovskite $CH_3NH_3PbI_{3-x}Cl_x$, Solid State Sci. 82 (2018) 19–23.

[55] D. Liu, M.K. Gangishetty, T.L. Kelly, Effect of $CH_3NH_3PbI_3$ thickness on device efficiency in planar heterojunction perovskite solar cells, J. Mater. Chem. A 2 (2014) 19873–19881.

[56] Q. Wang, Y. Shao, Q. Dong, Z. Xiao, Y. Yuan, J. Huang, Large fill-factor bilayer iodine perovskite solar cells fabricated by a low-temperature solution-process, Energy Environ. Sci. 7 (2014) 2359–2365.

[57] I. Levine, P.K. Nayak, J.T.-W. Wang, N. Sakai, S. Van Reenen, T.M. Brenner, S. Mukhopadhyay, H.J. Snaith, G. Hodes, D. Cahen, Interface-dependent ion migration/accumulation controls hysteresis in MAPbI3 solar cells, J. Phys. Chem. C 120 (30) (2016) 16399–16411.

[58] L.A.A. Pettersson, L.S. Roman, O. Inganäs, Modeling photocurrent action spectra of photovoltaic devices based on organic thin films, J. Appl. Phys. 86 (1) (1999) 487–496.

[59] G.F. Burkhard, E.T. Hoke, M.D. McGehee, Accounting for interference, scattering, and electrode absorption to make accurate internal quantum efficiency measurements in organic and other thin solar cells, Adv. Mater. 22 (30) (2010) 3293–3297.

[60] M. Liu, M. Endo, A. Shimazaki, A. Wakamiya, Y. Tachibana, Light intensity dependence of performance of lead halide perovskite solar cells, J. Photopolym. Sci. Technol. 30 (5) (2017) 577–582.

[61] A.K.K. Kyaw, D.H. Wang, V. Gupta, W.L. Leong, L. Ke, G.C. Bazan, A.J. Heeger, Intensity dependence of current–voltage characteristics and recombination in high-efficiency solution-processed small-molecule solar cells, ACS Nano 7 (5) (2013) 4569–4577.

[62] K. Tvingstedt, L. Gil-Escrig, C. Momblona, P. Rieder, D. Kiermasch, M. Sessolo, A. Baumann, H.J. Bolink, V. Dyakonov, Removing leakage and surface recombination in planar perovskite solar cells, ACS Energy Lett 2 (2) (2017) 424–430.

[63] W. Tress, M. Yavari, K. Domanski, P. Yadav, B. Niesen, J.P. Correa Baena, A. Hagfeldt, M. Graetzel, Interpretation and evolution of open-circuit voltage, recombination, ideality factor and subgap defect states during reversible light-soaking and irreversible degradation of perovskite solar cells, Energy Environ. Sci. 11 (2018) 151–165.

[64] A. Babayigit, J. D'Haen, H.-G. Boyen, B. Conings, Gas quenching for perovskite thin film deposition, Joule 2 (7) (2018) 1205–1209.

Dr. **Dong Zhang** studied material science at Shandong University in China and at Ulm University in Germany. He obtained his PhD degree in Photovoltaic Materials and Devices group at Delft University of Technology in the Netherlands. His PhD research topic was development of silicon heterojunction solar cells. Since 2013 he has joined the thin-film PV group at Energy research Centre of the Netherlands (ECN). Currently he is a research scientist at TNO-Solliance, focusing on development of high-efficiency hybrid tandem PV technologies.

Francesco Di Giacomo received his MSc degree in Materials Science from the Tor Vergata University in Rome. He did his Ph. D. in Electrical Engineering at the CHOSE lab (Tor Vergata) investigating the upscaling of perovskite solar cells (PSC) on flexible and rigid substrates. In 2015 he joined the Holst Centre – Solliance, working on the industrialization of PSC by means of sheet-to-sheet and roll-to-roll manufacturing and coordinating the activities on new materials and processes. He published more than 25 papers and filed 3 patents on this topic. In 2019 he joined the CHOSE lab as partner of the Espresso EU project.

Mehrdad Najafi earned his Ph.D. degree in Solid state Physics from the Shahrood University of Technology in 2015, the thesis was about synthesis and optical properties of metal oxides, while he pursued the scientific work on perovskite solar cells using the metal oxide layers at Zernike Institute for Advanced Materials, University of Groningen. Since 2016 he became a researcher at Solliance. He is focused on improving the efficiency and stability of perovskite solar cells for single junction and tandem application.

Sjoerd Veenstra has a passion for photovoltaics (PV). He received his PhD from the University of Groningen. Sjoerd stayed for several months at UCSB (intern) and Cornell University (visiting scientist). He started as a researcher working on organic solar cells at at the energy research centre of the Netherlands (ECN). In 2011 he moved to Eindhoven (NL) to join the thin film PV activities (including OPV) of Solliance. Solliance shifted focus from OPV to perovskite solar cells at the end of 2014. Since 2018 he works for TNO and leads the perovskite solar cell program of Solliance.

Damian Głowienka received his PhD degree in physics from Gdańsk University of Technology. His PhD research topic was focused on device physics of perovskite and organic solar cells. He is currently a postdoctoral fellow at TNO-Solliance. His research focuses on recombination phenomena in perovskite solar cells with both experimental and computational methods.

Jędrzej Szmytkowski received his MSc, PhD and DSc (habilitation) degrees in physics from Gdańsk University of Technology, Gdańsk, Poland. He worked as a postdoctoral researcher in Karlsruhe Institute of Technology (Germany), University of Saskatchewan (Canada) and University of Florida (USA). Currently, he is an associate professor at Faculty of Applied Physics and Mathematics in Gdańsk University of Technology. His research interests include molecular physics, organic electronics and photovoltaics.

Yulia Galagan is a Senior Scientist at TNO/Solliance. She received her PhD in chemistry in 2002 from Kyiv University. She was a post-doctoral researcher at National Taiwan University, and in 2008 she joined TNO/Holst Centre. Her research interests are focused on organic and perovskite-based opto-electronics electronics, including perovskite solar cells. Currently, Yulia Galagan is a group leader responsible for scale-up technologies for roll-to-roll manufacturing of perovskite-based photovoltaics.